https://doi.org/10.5194/acp-2020-639
Preprint. Discussion started: 30 July 2020

Atmospheric Chemistry and Physics Discussions

Analysis of atmospheric ammonia over South and East Asia based on the MOZART-4 model and its comparison with satellite and surface observations

Pooja V. Pawar[1*], Sachin D. Ghude[1], Chinmay Jena[1], Andrea Móring[2,7], Mark A. Sutton[2], Santosh Kulkarni[3], Deen Mani Lal[1], Divya Surendran[4], Martin Van Damme[5], Lieven Clarisse[5], Pierre-François Coheur[5], Xuejun Liu[6], Wen Xu[6], Jize Jiang[7], and Tapan Kumar Adhya[8]

[1]Indian Institute of Tropical Meteorology (IITM), Pune, 411008, India
[2]Centre for Ecology & Hydrology (CEH), Edinburgh, EH26 0QB, UK
[3]Centre for Development of Advanced Computing, Pune, 411008, India
[4]Indian Meteorological Department (IMD), Pune, 411005, India
[5]Université libre de Bruxelles (ULB), Spectroscopy, Quantum Chemistry and Atmospheric Remote Sensing (SQUARES), Brussels, B-1050, Belgium
[6]College of Resources and Environmental Sciences, National Academy of Agriculture Green Development, China Agricultural University, Beijing 100193, China
[7]The University of Edinburgh, Scotland, EH8 9AB, UK
[8]Kalinga Institute of Industrial Technology, Bhubaneshwar, 751016, India

Correspondence to: Sachin D. Ghude (sachinghude@tropmet.res.in)

Abstract. Limited availability of atmospheric ammonia (NH_3) observations, limits our understanding of controls on its spatial and temporal variability and its interactions with ecosystems. Here we used the Model for Ozone and Related chemical Tracers (MOZART-4) global chemistry transport model and the Hemispheric Transport of Air Pollution version-2 (HTAP-v2) emission inventory to simulate global NH_3 distribution for the year 2010. We present a first comparison of the model with monthly averaged satellite distributions and limited ground-based observations available across South Asia. The MOZART-4 simulations over South Asia and East Asia are evaluated with the NH_3 retrievals obtained from the Infrared Atmospheric Sounding Interferometer (IASI) satellite and 69 ground based monitoring stations for air quality across South Asia, and 32 ground based monitoring stations from the Nationwide Nitrogen Deposition Monitoring Network (NNDMN) of China. We identify the northern region of India (Indo-Gangetic Plain, IGP) as a hotspot for NH_3 in Asia, both using the model and satellite observations. In general, a close agreement was found between yearly-averaged NH_3 total columns simulated by the model and IASI satellite measurements over the IGP, South Asia (r=0.85) and North China Plain (NCP), of East Asia (r=0.88). However, the MOZART-4 simulated NH_3 column is substantially higher over South Asia than East Asia, as compared with the IASI retrievals, which show smaller differences. Model simulated surface NH_3 concentrations indicate smaller concentrations in all seasons than surface NH_3 measured by the ground based observations over South and East Asia, although uncertainties remain in the available surface NH_3 measurements. Overall, the comparison of East Asia and South Asia using both MOZART-4 model and satellite observations showed smaller NH_3 columns in East Asia compared with South Asia for comparable emissions, indicating rapid dissipation of NH_3 due to secondary aerosol formation, which can be explained by larger emissions of acidic precursor gases in East Asia.

https://doi.org/10.5194/acp-2020-639
Preprint. Discussion started: 30 July 2020

Atmospheric Chemistry and Physics Discussions

1 Introduction

Gaseous pollution due to various forms of nitrogen emissions plays an important role in environmental processes. Specifically, ammonia (NH_3) emitted from various agricultural activities, such as use of chemical fertilizers, animal farming, etc., together with nitrogen oxides (NO_x) is one of the largest sources of reactive nitrogen (N_r) emission to the atmosphere. Ammonia has great environmental implications due to its substantial influence on the global nitrogen cycle and associated air pollution, ecosystem and on public health (Behera et al., 2013; Liu et al., 2017b; Zhou et al., 2016). Ammonia is a key precursor in aerosol formation, as the reactions in the atmosphere lead to an increase in different forms of sulphates and nitrates that contribute in secondary aerosol formation (Pinder et al., 2007, 2008). South and East Asia together accounted for an estimated 64 % of the total amount of NH_3 emissions during 2000-2014 (Xu et al., 2018). Emissions of NO_x and NH_3 are increasing substantially over South Asia (Sutton et al., 2017), which contributes to increase in particulate mass loading, visibility degradation, acidification and eutrophication (Behera et al., 2013; Ghude et al., 2008, 2013, 2016). Asia is responsible for the largest share of global NH_3 emissions (Janssens-Maenhout et al., 2012). Further increase in NH_3 emission will increase its negative impacts and societal cost (Sutton et al., 2017).

Recent study based on Infrared Atmospheric Sounding Interferometer (IASI) satellite measurements show very high concentration of NH_3 over Indo-Gangetic Plain (IGP) and North China Plain (NCP) which were mainly related to agricultural (Van Damme et al., 2014a, 2014b, 2015) and industrial activity (Clarisse et al., 2019; Van Damme et al., 2018). The seasonality was shown to be more pronounced in the northern hemisphere, with peak columns in spring and summer season (Van Damme et al., 2014a). Emission estimates provided by EDGAR v4.2 emission inventory suggests that globally about 49.3 teragram (Tg) of NH_3 was emitted in the atmosphere in 2008 out of which agricultural soils contributed 58 %, manure management contributed 21 % and 2 % agricultural burning (Sutton et al., 2013).

In India, around 50 % of total NH_3 emissions is estimated from the fertilizer application and remaining from livestock and other NH_3 sources (Aneja et al., 2011; Behera et al., 2013). However, there are large uncertainties in emissions of ammonia, its deposition to surface, chemistry and transport (Sutton et al., 2013; Zhu et al., 2015). In fertilizer application, urea contributes more than 95 % to the fertilizer demand and consumption (Fertlizer Association of India annual report 2018-19), and contributes more than 90 % of NH_3 emissions (Sharma et al., 2008). India is currently the second largest consumer of fertilizers after China, and fertilizer usage is bound to increase with further intensification of agriculture and the fertilizer input of India is expected to be doubled by 2050 (Alexandratos and Bruinsma, 2012).

In this study, we examined the spatio-temporal variability of atmospheric NH_3 over Asia (South and East Asia) and focus on two hotspots regions of ammonia, the Indo-Gangetic Plain (IGP) and the North China Plain (NCP). The approach for this study is a combination of simulations using chemical transport modelling, satellite observations and *in-situ* ammonia measurements over South Asia (69 stations) and East Asia (32 stations). The analysis applies the Model for Ozone and Related chemical tracers (MOZART-4) driven by priori ammonia emissions based on Hemispheric Transport of Air Pollution version-2 (HTAP-v2) emission inventory. It applies HTAP-v2 data for emissions to produce estimated total columns of NH_3 and aerosol species for the year 2010 over Asia. Model simulations were evaluated and compared with NH_3 data from IASI (over South and East Asia) and selected ground-based observations (noted above). In addition to the regional comparison,

https://doi.org/10.5194/acp-2020-639
Preprint. Discussion started: 30 July 2020

Atmospheric Chemistry and Physics Discussions

we examine why certain emission hotspot regions in East Asia show lower NH_3 total columns compared with similar hotspot regions in South Asia, when analyzed with both model and satellite observations.

2. Data and methodology

2.1 MOZART-4 model

The global chemical transport model MOZART-4 has been employed in this study to conduct a year-long (2010) simulation of NH_3 and other trace gases over Asia using the updated HTAP-v2 emission inventory (Janssens-Maenhout et al., 2015). These simulations were earlier performed to meet the objectives of Task Force on Hemispheric Transport of Air Pollution, phase 2, multi-model experiments (Surendran et al., 2015; Surendran et al., 2016). The model domain covers entire globe at a horizontal grid resolution of 1.9° × 2.5° and 56 vertical levels from the surface up to 1 hectopascal (hPa). MOZART-4 takes into account surface emissions, convection, advection, boundary layer transport, photochemistry, and wet and dry deposition. The model simulations were driven by the input meteorological data set of 1.9° × 2.5° resolution from Modern Era Retrospective-analysis for Research (MERRA) and Applications of the Goddard Earth Observing System Data Assimilation System (GEOS-DAS). Model simulations were performed for the complete year of 2010 (1 January 2010 to 31 December 2010) and its outputs were saved every 6h (4 time steps each day) with a spin up time of six months (1 July 2009 to 31 December 2009). MOZART-4 includes 157 gas-phase reactions, 85 gas-phase species, 39 photolysis and 12 bulk aerosol compounds (Emmons et al., 2010). Dry deposition of gases and aerosols were calculated online according to the parameterization of Wesely (1989) and wet deposition of soluble gases were calculated as described by the method of Emmons et al. (2010). The ammonium nitrate distribution is determined from NH_3 emissions and the parameterization of gas/aerosol partitioning by Metzger et al. (2002), which is a set of approximations to the equilibrium constant calculation (Seinfeld et al., 1998), based on the level of sulphate present. Biomass burning emissions of a wide range of gaseous components, including NH_3, SO_2 and individual volatile organic compounds were provided from the Global Fire Emission Database (GFED-v3), determined by scaling the GFED CO_2 emissions by the emission factors provided on 1.9° × 2.5° grid resolution (Emmons et al., 2010).

2.2 Emission inventory (HTAP-v2)

The HTAP-v2 bottom-up database is used in this study as an input for anthropogenic emissions of NH_3 for the year 2010 (Janssens-Maenhout et al., 2015). HTAP-v2 dataset is embedded with the activity data as per harmonized emission factors, international standards, and gridded emissions with global proxy data. It includes important point sources providing high spatial resolution and emission grid maps with global coverage. This dataset consists of monthly mean NH_3 emission maps with $0.1^{\circ} \times 0.1^{\circ}$ grid resolution for the year 2010. The HTAP-v2 dataset is compiled using various regional gridded emission inventories by Environmental Protection Agency (EPA) for USA and Environment Canada for Canada, European Monitoring Evaluation Programme (EMEP) and Netherlands Organisation for Applied Scientific Research for Europe, and Model Inter comparison Study in Asia (MICS Asia) for China, India and other Asian countries. The emissions Database for Global Atmospheric Research (EDGARv4.3) is used for the rest of the world (mainly South-America, Africa, Russia and Oceania). The 'MICS Asia' dataset incorporated into the HTAP-v2 dataset includes an anthropogenic

https://doi.org/10.5194/acp-2020-639
Preprint. Discussion started: 30 July 2020

Atmospheric Chemistry and Physics Discussions

emission inventory developed in 2010 (Li et al., 2015), which incorporates several local emission inventories, including the Multi-resolution Emission Inventory for China (MEIC), NH_3 emission inventory from Peking University (Huang et al., 2012) and Regional Emission inventory in Asia version 2.1 (REAS2.1) (Kurokawa et al., 2013) for areas where local emission data are not available. A detailed description on HTAP-v2 datasets can be found in Janssens-Maenhout et al. (2015).

For this study, we used emissions from five important sectors, such as, agricultural, residential, energy, transport and industries for the year 2010. These emissions also includes natural emissions such as soil from the Community Earth System Model (CESM), and biomass burning from the Global Fire Emission Database (GFED-v3) (Randerson et al., 2013). All these emissions are re-gridded to $1.9^{\circ} \times 2.5^{\circ}$ to match the model resolution.

The spatial distribution of the total NH_3 emissions over Asian region is shown in Fig. 1. It shows the highest emissions over both South and East Asia, especially over the IGP and NCP region (shown with black box in Fig. 1). Agricultural sector is the main contributor to NH_3 emission, including management of manure and agricultural soils (application of nitrogen fertilizers, including animal waste). It also includes emissions from livestock, crop cultivation excluding emissions from agricultural waste burning and savannah burning (Janssens-Maenhout et al., 2015). Minor contributions from the residential sector are also observed for the Asian countries due to use of fossil fuel (cow dung and coal burning) which is also included in the emissions. Spatial proxies such as population density, road networks, and land use information have been used to allocate area of emission sources. For the REAS2 emission inventory over India, the agricultural sector follows spatial proxy of total population (Li et al., 2017). The use of this approach is expected to be the main source of spatial uncertainty in the estimated NH_3 emissions to the extent that total human population is only approximately correlated with spatial distribution of fertilizer use and livestock numbers. Seasonal variation of average NH_3 emission over the IGP and NCP region for Anthropogenic (HTAP-v2), biomass burning (GFED-v3) and Soil emission (CESM) is shown in Fig. 2. Anthropogenic NH_3 emissions do not show any strong seasonal variability over the IGP region however over the NCP region, NH_3 emissions show strong seasonality with peak emissions between May-September months. It can be seen that the magnitude of peak emissions is two times more over the NCP region than IGP region. On the other hand, seasonality in biomass burning NH_3 emissions is strong over the IGP region, which shows highest emissions in the spring season (MAM). Also, contribution of NH_3 emissions from the IGP region is significantly higher compared to NCP region during peak burning season, but the magnitude of biomass burning emission is six times lower compared to the magnitude of anthropogenic emissions.

2.3 Satellite NH_3 observations

We have used ANNI-NH_3-v2.2R-I dataset from IASI satellite for the year 2010 (Van Damme et al., 2017) gridded at the horizontal resolution of the model (1.9° × 2.5°). Only morning overpasses at 09:30 am are considered in this study, as these are more sensitive to NH_3 (Clarisse et al., 2010; Van Damme et al., 2014a). IASI is a suitable tool for evaluation of regional and global models due to its relatively high spatial and temporal sampling (Whitburn et al., 2016). More details about IASI satellite and NH_3 data product is given in Clerbaux et al. (2009), Van Damme et al. (2017) and Whitburn et al. (2016).

https://doi.org/10.5194/acp-2020-639
Preprint. Discussion started: 30 July 2020

Atmospheric Chemistry and Physics Discussions

2.4 Ground based observations

To evaluate model performance in South Asia, we used hourly NH_3 measurements from the air quality monitoring station network operated by Central Pollution Control Board (CPCB) across India. CPCB follows a program for sampling of ambient air quality as well as weather parameters measurements. An automatic analyzer (continuous) method is adopted at each monitoring location. NH_3 is measured by the chemiluminescence method as NO_x following oxidation of NH_3 to NO_x. In this approach, NH_3 is determined from the difference between NO_x concentration with and without inclusion of NH_3 oxidation (CPCB, 2011). The quality assurance and control process followed for these air quality monitoring instruments is given in CPCB (2020) report. Surface observations of NH_3 are taken from 69 different stations in South Asia. The details of these monitoring locations are given in Table S1 (in the Supplement) and the geographical locations are shown in Fig. 3. Out of these stations thirty five locations in Delhi, six in Bangalore city, four in Hyderabad, and two in Jaipur city are averaged to get single value for the same geographical location and the remaining 22 locations are considered independently representing 26 respective cities. Hourly NH_3 concentrations (in μg m^{-3}) used in the study are for the duration of 2016 to 2019. Given the presence of relatively high NOx concentrations, especially at urban locations, it is recognized that the measurement of NH_3 by difference (i.e., between NO_x and NO_x plus oxidized NH_3), is a potentially significant source of uncertainty. Future measurement inter-comparisons are planned (rescheduled from 2020 to 2021 because of COVID-19) to allow the chemiluminescence method as used in the Indian network to be compared with a range of other NH_3 measurement methods. To further evaluate model performance over East Asia, we used monthly mean NH_3 measurements from the 32 stations of the Nationwide Nitrogen Deposition Monitoring Network (NNDMN) of China, operated by China Agricultural University. The details of these monitoring locations are given in Table S2 (in the Supplement) and the geographical locations are shown in Fig. 3. Monthly mean NH_3 concentrations (in μg m^{-3}) used in the study are for the duration of 2010 to 2015. Ambient concentrations of gaseous NH_3 were measured using an active Denuder for Long-Term Atmospheric sampling (DELTA) system. More detail about the data product is given by Xu et al. (2019).

3. Results and Discussion

3.1 Annual mean NH_3 total columns over South Asia

Yearly-averaged 2010 distribution of NH_3 total columns over Asia simulated by MOZART-4 model and also retrieved with IASI instrument are shown in Fig. 4a and 4b. The total NH_3 columns simulated by the model show high Tropospheric Vertical Column Densities (TVCDs) of about 0.5-7×10^{16} molecules cm^{-2} over IGP region of India compared to any other regions of Asia. This may reflect the larger range of NH_3 column values for the South Asian model domain, with both more polluted and cleaner conditions. These high TVCDs values coincide with the high fertilizer-N and livestock numbers, as scaled according to human population density in Fig. 1.

Spatial differences between model simulated data and satellite data for NH_3 total column distribution are shown in Fig. 4c. On a quantitative level, the MOZART-4 model is found to overestimates the NH_3 total column compared with IASI by 1-4×10^{16} molecules cm^{-2} over South Asia, especially over northeast India and Bangladesh. Conversely, the MOZART-4 model underestimates NH_3 in comparison with IASI over the arid

https://doi.org/10.5194/acp-2020-639
Preprint. Discussion started: 30 July 2020


Atmospheric Chemistry and Physics Discussions

region of north western India (state of Rajasthan adjacent to Pakistan) and centering on Pakistan. There are several possible reasons for the spatial differences shown in Fig. 4c, including: a) uncertainties in the mapped NH_3 emissions data (e.g., between Afghanistan, Bangladesh, India and Pakistan, due to different relationships between human population and livestock/fertilizer activities); b) uncertainties related to turbulent mixing and dispersion (this may affect both the simulations in MOZART-4 and the assumed vertical profiles for the IASI retrievals); and c) uncertainties related to precipitation scavenging of ammonia and ammonium, noting that the eastern part of the IGP is substantially wetter than the western part.

According to Fig. 1, the magnitude of NH_3 emissions over NCP is similar to IGP. By contrast, much smaller TVCDs of the NH_3 columns are estimated by MOZART-4 and IASI over NCP compared with IGP. The MOZART-4 and IASI estimates are found to be in close agreement, with slightly smaller values estimated by MOZART-4. The possible reasons for the difference in NH_3 concentrations in IGP and NCP are discussed in Sect. 3.4. The relationship between modelled and IASI retrieved NH_3 total columns are further analysed in terms of scatter plots in Fig. 5a and 5b, over IGP region of South Asia (20°N-32°N, 70°E-95°E) and NCP region of East Asia (30°N-40°N, 110°E-120°E) (rectangular areas shown in Fig. 1). Correlation coefficients (r) between model and satellite observed annual mean total columns over IGP and NCP are found to be 0.85 and 0.88 respectively for 2010. This indicates that spatial variability in simulated NH_3 by the model and satellite observation is in closer agreement, both over IGP and NCP region. The Model simulated NH_3 gives larger values over IGP region (Normalised Mean Bias (NMB) = 42 %) as well as over entire South Asia (NMB = 49 %). Whereas over the NCP region (NMB = -20 %) and entire East Asia (NMB = -13 %), the model gives values which are smaller than IASI. Other statistical indicators are summarised in Table 1. Larger estimates of NH_3 columns from an atmospheric Chemistry Transport Model (CTM) compared with IASI was also found in an earlier study for South Asia (Clarisse et al., 2009).

The overall higher value of the model simulated NH_3 over South Asia compared with IASI could be due to the combination of the uncertainties in both approaches. This includes uncertainties in emissions from the HTAP-v2 datasets used for the model simulations, inaccurate modelling of the chemistry in MOZART-4, errors in dry and wet deposition schemes used in the model, and biases inherent to infrared satellite remote sensing. For IASI, firstly, only cloud-free satellite scenes are processed, which could result in missing partly some of the NH_3 values during cloudy periods and biomass burning events. Secondly, NH_3 vertical columns retrieved from the IASI observations are actually sampled around 09:30 local time which does not represent exact daily average NH_3 concentrations as simulated by the MOZART-4 model (Clarisse et al., 2009). Finally, the retrieval of NH_3 from infrared satellites is sensitive to inaccuracies in the temperature profile, and biases in the IASI L2 temperature profiles can result in biases in the retrieved NH_3 (Whitburn et al., 2016). The HTAP-v2 dataset use proxy values for agricultural activities (i.e., distributed by human population) instead of actual values for field fertilizer application and livestock excretion over the South Asia. This could also result in additional uncertainty of NH_3 emissions from the agricultural activities. In MOZART-4 chemistry, nitrate is absent hence errors can be associated in dry and wet deposition scheme which can result in overestimation (Emmons et al., 2010). Further work is on-going to integrate NH_3 emissions inventories for different countries in South Asia based on national datasets, which should allow the emissions related uncertainties to be reduced in future. Similarly, slight underestimation over East Asia might originates from the country specific emission inventory used for China (Huang et al., 2012) in MOSAIC HTAP-v2 emission inventory and the limitations discussed above.

https://doi.org/10.5194/acp-2020-639
Preprint. Discussion started: 30 July 2020

Atmospheric Chemistry and Physics Discussions

3.2 Seasonal variability of NH_3 total columns

Figure 6 shows the model (left) and IASI satellite (middle) seasonal distributions of NH_3 total columns over Asia. These seasons are represented as 3-month periods: Winter, December-January-February (DJF, first row), Spring, March-April-May (MAM, second row), Summer, June-July-August (JJA, third row), and Autumn, September-October-November (SON, fourth row). It can be seen in Fig. 6, that there is larger seasonal variation in IASI NH_3 total columns while MOZART-4 presents limited seasonality as in South Asia compare to better seasonal variation estimated in East Asia, as shown by both IASI and the MOZART-4 model. In general, during autumn, spring, summer and winter seasons MOZART-4 shows higher NH_3 total column compared with IASI estimates over most of South Asia. However, this difference is more pronounced during autumn (SON) and winter (DJF) seasons (Fig. 6; Right).

We have seen that (Fig. 2) anthropogenic emission of NH_3 is nearly same in all months and biomass burning has peak during MAM over South Asia in the MOZART-4 model. Whereas, seasonality is better represented in NH_3 emission for East Asia. Major drivers in anthropogenic NH_3 seasonal variation include differences in management and timing of fertilizer, which may not be well represented in the emission over South Asia (Janssens-Maenhout et al., 2012). This can be expected to have the direct effect on NH_3 total column over South Asia. It is recognized that NH_3 emission can be strongly affected by both short term meteorological variation and longer term climatic differences (Sutton et al., 2013). This means that larger NH_3 emissions may be expected in warm summer conditions than in winter, which is well represented in the emission estimate (soil) over both East and South Asia (Fig. 2). This may partly explain why IASI shows larger summertime NH_3 columns in both South Asia and East Asia than MOZART-4. However, magnitude of these emissions is expected to be smaller in comparison with anthropogenic emissions. Additional driver in NH_3 seasonal variation include meteorological variation. For example, strong subsidence, lower temperature and lighter winds over South Asia in the autumn and winter months prevent venting of low altitude pollution to the higher altitudes. This means that emitted air pollutants tend to accumulate close to the source region in winter time conditions (Ghude et al., 2010, 2011), which is reflected in the higher wintertime values of MOZART-4. Considering the comparison of IGP with NCP, accumulation of pollutants in the boundary layer is more pronounced over IGP region due to flat land topography, and it is more during winter than the autumn months (Surendran et al., 2016). We saw that simulated mean Planetary boundary layer height (PBLH) is lower by about approximately 400 m and winds are lighter in winter months, compared to summer months, over South Asia, and particularly over IGP region (Fig. S1 in the Supplement). Similarly, NH_3/NH_4 ratio is higher (Fig. S2 in the Supplement) and dry and wet deposition (Fig. S3 and S4 in the Supplement) of NH_3 is lower over IGP in winter month compared to summer months. Also, sowing of wheat crop over IGP involves higher rate of fertilizer application during peak winter month (Sharma et al., 2014) that release significant quantity of NH_3 into the atmosphere. However, this seasonality is largely missing in the emissions (Fig. 2 (top, left)) indicating that higher MOZART-4 NH_3 is largely driven by the winter-time meteorology over this region. Limited sensitivity and sampling of IASI measurements in autumn and winter seasons could be one of the reasons for large differences ($1\text{-}4\times10^{16}$ molecules cm^{-2}) between MOZART-4 and IASI (Van Damme et al., 2014a). During spring season, MOZART-4 reflects widespread NH_3 total column from the entire Indian land mass and IASI observations does capture increase in NH_3 total column at least for seasonal mean cycle (Fig. 7a). This seasonal maximum in NH_3 total

https://doi.org/10.5194/acp-2020-639
Preprint. Discussion started: 30 July 2020

Atmospheric Chemistry and Physics Discussions

column identified both in IASI and MOZART-4 over South Asia can be explained by the two factors: Meteorology factor and biomass burning emissions. Volatilization of NH_3 enhances with increase in temperature (Sutton et al., 2013), hence higher temperature during this drier periods over IGP partly enhances NH_3 emission to the environment which is also evident from the soil NH_3 emissions in Fig. 2 (bottom). In the Indian region, emissions from the biomass burning (crop-residue burning) peaks in March to May (Jena et al., 2015) and emission of NH_3 from biomass burning is maximum during this period (Fig. 2 (middle)). However, MOZART-4 estimates smaller NH_3 total columns compared with IASI over Myanmar, Laos and Thailand during the period March-May (Fig. 6 (right)). This period is estimated to be associated with large scale forest fires (and open crop burning) (Chan, 2017; Wu et al., 2018; Zheng et al., 2017), the effect of which appears to be underestimated in the MOZART-4 simulations. It suggests that the Global Fire Emissions Database (GFED-v3) used in this study is low over this region agreeing with Zhang et al. (2020) and Huang et al. (2013). It is interesting to note from Fig. 6 (right) that during spring the difference between modelled and observed column NH_3 is smaller over the IGP region compared with the winter season. Heating of the landmass due to large solar incidence suppresses the wintertime subsidence over the IGP and leads to deeper boundary layer. It can be seen that (Fig. S1 in the Supplement) the average PBLH is about 400 m deeper during summer compared to winter over IGP. In addition, significant transport of the boundary pollution in the mid and upper troposphere takes place due to enhanced convective activities and large scale vertical motion (Lal et al., 2014; Surendran et al., 2016). Vertical motion associated with the convective activities is expected to redistribute the NH_3 concentration in the column, which leads to more NH_3 at the higher altitudes where detection sensitivity of the satellite is more than that at the surface (Clarisse et al., 2010). As a result, more NH_3 gets detected by the satellite and we see less difference between observations and model over the IGP. This may also partly explain the higher IASI estimates of NH_3 column for summertime prior to the monsoon season. However, this hypothesis needs to be tested with higher sensitivity experiments as a part of future work. During the monsoon season (JJA) (Fig. 6 (right)) and summer, IASI-NH_3 total columns are larger than the MOZART-4 estimates over north-western arid region of South Asia, where monsoon rainfall is lowest (less than 30 cm). On the other hand, NH_3 columns estimated by IASI are lower in the North-western IGP than the MOZART-4 simulations.

Figure 7 shows the comparison between IASI and modelled monthly time series of NH_3 total columns over IGP (20°N-32°N, 70°E-95°E) and NCP (30°N-40°N, 110°E-120°E), respectively (rectangular areas shown on Fig. 1). We found a better consistency between modelled and measured seasonal NH_3 total column over NCP than IGP. Monthly NH_3 columns over the IGP show bimodal distribution in the model. However, IASI does not show such bimodal variation. Seasonal statistics show large normalised mean bias (65 %) and poor correlation (r= 0.47) between model and IASI. The bimodal distribution in NH_3 total columns is partly driven by the biomass burring emissions, which show major peak in spring and another small peak in autumn (Fig. 2 (middle)), and partly by the meteorology as discussed in the previous section. During monsoon months (JJA), when South Asia receives significant rainfall all over, model simulations present lower NH_3 total column, which is not seen in the IASI observations and also in the surface observations (Fig. 7a and 8b) over IGP. The reason for this discrepancy may be related with the flat NH_3 emission over South Asia (Fig. 2). Usually large amount of fertilization application is expected during the warm month of June and July in the IGP which is not represented in the HTAP-v2 emissions and therefore lower values in the model during monsoon month is mostly driven by the model meteorology. Lower values observed during monsoon season in general are attributed to increase wet

https://doi.org/10.5194/acp-2020-639
Preprint. Discussion started: 30 July 2020


Atmospheric Chemistry and Physics Discussions

scavenging of NH_3 due to monsoon rain (Fig. S4 (left) in the Supplement) and influx of cleaner marine air from the Bay of Bengal and Arabian Sea through south-easterly and south-westerly wind (Ghude et al., 2008). On the other hand, monthly variation in IASI NH_3 total columns over East Asia is found to be captured well by the model (Fig. 7b) and seems to follow the variation observed in the anthropogenic NH_3 emission (Fig. 2), except for the month of July where IASI estimates substantially higher NH_3 total columns than the model. The reason for this peak in the IASI data for July may be related to urea fertilizer application in warm July conditions (see temporal course of Enhanced Vegetation Index (Li et al., 2014)), which seems to be not represented well in the HTAP-v2 emissions. The overall statistics show slight good correlation (r=0.53) between observed and simulated NH_3 columns and small normalised mean bias (NMB = -30 %).

3.3 Comparison between surface NH_3 measurements and simulated NH_3 concentrations in South and East Asia

To evaluate modelled surface NH_3 concentrations in South Asia, we have used NH_3 surface measurements from 69 monitoring locations over India for the years from 2016 to 2019. As 2010 data was not available, we make the hypothesis that measurement from 2016-2019 can be considered as representative from what have been measured in 2010. Out of these stations thirty five locations in Delhi, six in Bangalore city, four in Hyderabad, and two in Jaipur city are averaged to get singe value for the same geographical location and the remaining 22 locations are considered independently representing 26 respective cities. Due to the lack of ground-based measurements performed in 2010, the following comparison will mainly be qualitative, although it is estimated that the main spatial features of Indian agriculture and NH_3 emissions will be consistent between 2010 and 2016-2019. As per the RCP 8.5 (Kumar et al., 2018) NH_3 emission from South Asia is expected to increase by less than 20 % from 2010 to 2020. Assuming a linear relationship between emission and surface concentration, it is expected that NH_3 concentrations could be higher by about 10-15 % in 2016 to 2019.

It is interesting to note that the correlation between annual and monthly mean MOZART-4 simulated and measured NH_3 concentration (r=0.82 and r=0.62) is better than the comparison between MOZART-4 and IASI for South Asia (Fig. 8). However, the MOZART-4 has systematically smaller estimated NH_3 concentrations compared with the ground based measurement network (NMB = -47 %). It should be noted that most of the monitoring stations are situated in urban regions (cities) of India and therefore represents the urban environment, which may have locally higher NH_3 concentrations due to traffic and human activities (Sharma et al., 2014). Since the MOZART-4 model is run relatively at coarse (1.9° × 2.5°) grid resolution the emissions may not capture the true variability in emissions at city scale. These surface NH_3 sites are influenced by local emissions that are therefore not resolved by the MOZART-4 model. Therefore, when comparing coarse-scale models to observations, the model may have difficulties in resolving local scales effects (Surendran et al., 2015). Until the planned further evaluation of the chemiluminescence monitoring method for ammonia (measured by difference with NOx) is evaluated (as noted in Sect. 2.4), it is not possible to be certain the extent to which possible uncertainties in the measurement method contribute to the differences shown in Fig. 8b. While noting these uncertainties, it is worth noting that the ground based NH_3 observation network confirms the occurrence of higher ground-level NH_3 concentrations in autumn and winter, as simulated using MOZART-4 using the HTAP-v2 emissions inventory (Fig. 8b).

Comparison of Fig. 7a and 8b shows that the time course of ground level NH_3 concentrations (as estimated by MOZART-4) is significantly different to the time course of total NH_3 column (as also estimated by MOZART-

https://doi.org/10.5194/acp-2020-639
Preprint. Discussion started: 30 July 2020


Atmospheric Chemistry and Physics Discussions

4). Whereas the total column is largest in the summer (reflective of deeper atmospheric mixing and recirculation), and the ground level concentrations are largest during winter. Although it is not easy to use the IASI data to infer ground level NH_3 concentrations, the stronger summer maximum of IASI (Fig. 7a) compared with MOZART-4, suggests that IASI would be in less close agreement with the ground based measurement network than MOZART-4 (Fig. 8b). While recognizing uncertainties in this interpretation, the key point is that large NH_3 columns estimated by IASI for May-July are not reflected in the ground-based NH_3 measurements from the Indian monitoring network.

Figure 9 shows the comparison between monthly mean (from 2010 to 2015 observations) NH_3 surface measurements from 32 monitoring locations over China and modelled surface NH_3 concentrations from the same location over East. Similar to South Asia the MOZART-4 has systematically smaller estimated NH_3 concentrations compared with the ground based measurement network (NMB = -44 %) over East Asia. Figure 9b shows maximum NH_3 concentration occurred in summer (JJA) denotes agreement with IASI measurements. Other statistical indicators are summarised in Table 2. High NH_3 concentration from ground based measurements during JJA is consistent with the higher HTAP-v2 emissions (Fig. 2) which is also reported in other similar study (Huang et al., 2012). This implies that the NH_3 emissions may play a vital role in determining the seasonal pattern of the ground NH_3 concentrations. Summer peak may originate from fertilizer application, livestock emissions and volatilization of NH_3 which is enhanced in higher temperature (Liu et al., 2017a).

3.4 Why were NH_3 total columns low over high NH_3 emission over East Asia compared to high NH_3 emission region of South Asia?

Fine-scale details of the NH_3 emissions over Asia in Fig. 1 and 2 clearly revealed larger emission values in areas where there is intensive agricultural management. This is the case especially in the NCP and IGP (Fig. 1, shown with box). Earlier emission estimates suggest that fertilizer application and livestock contribute 2.6 Tg per year (yr^{-1}) and 1.7 Tg yr^{-1} NH_3 emissions respectively from South Asia (Aneja et al., 2011). Over South Asia, urea accounts for emissions of 2.5 Tg yr^{-1} which contributes to 95 % of the fertilizer emission, and 58 % of total estimated agricultural emissions (Fertlizer Association of India annual report 2018-19). For East Asia, livestock manure management accounts for approximately 54 % (5.3 Tg yr^{-1}) of the total emissions and fertilizer application accounts for 33 % (3.2 Tg yr^{-1}) emissions, with 13 % of emissions from other sources. Combined the model areas for NCP and IGP (as shown in Fig. 1) accounts for ~45 % of the NH_3 emitted from fertilization in East Asia and South Asia (Huang et al., 2012).

We find that satellite observations show larger NH_3 columns over IGP than over similar higher emission regions of NCP. However, in addition, we also find that the MOZART-4 model is able to capture this contrasting columnar NH_3 levels between IGP and NCP. This indicates that the difference between IGP and NCP is unrelated to differences between the mosaic of emissions over South Asia and East Asia in HTAP-v2 and similarly not related to uncertainties in satellite retrievals. Instead, the analysis from MOZART-4 demonstrates that the difference can be explained by differences in atmospheric chemistry between the two regions, linked to higher SO_2 and NO_x emissions in the NCP than in the IGP.

As ammonia is a highly alkaline gas with an atmospheric lifetime usually of few hours (and rarely a few days) (Dammers et al., 2019), it readily reacts with acid present in the atmosphere to form aerosols, which are eventually deposited to the earth's surface by either dry or wet deposition processes (Fig. S3 and S4 in the

https://doi.org/10.5194/acp-2020-639
Preprint. Discussion started: 30 July 2020

Atmospheric Chemistry and Physics Discussions

Supplement). In the atmosphere, ammonia therefore reacts rapidly with atmospheric sulphuric acid (H_2SO_4), nitric acids (HNO_3) and hydrochloric acid (HCl) to contribute to ambient levels of fine particles, forming ammonium sulphate, ammonium nitrate and ammonium chloride. Following reaction (R1) and (R2)

$$NH_{3(g)} + HNO_{3(g)} \leftrightarrow NH_4NO_{3(s)} \quad \text{(R1)}$$

$$2NH_{3(g)} + H_2SO_{4(g)} \leftrightarrow (NH_4)_2SO_{4(s)} \quad \text{(R2)}$$

In the atmosphere, ammonium ion (NH_4^+) as an aerosol is estimated to have a lifetime of about 1–15 days (Aneja et al., 1998), though this is obviously dependent on the amount of atmospheric acids (Seinfeld and Pandis, 2012). In addition to the large fertilizer application and livestock management activities which are characteristic of both IGP and NCP, industrial and transportation activities are higher over the NCP (China) which also results in higher emission of NO_x and SO_2 over NCP compared with IGP (Zhao et al., 2013). Ammonia has greater affinity towards oxides of sulphur, hence it first reacts to form ammonium sulphate, and then the remaining ammonia further reacts to form ammonium nitrate (Seinfeld et al., 1998). The differences in the secondary aerosol formation over NCP and IGP are compared by considering the MOZART-4 model estimates of volume mixing ratio (VMR) in parts per billion ($\times 10^9$ ppb) of total sulphate, ammonium, ammonium nitrate at surface and total column of NO_x (Fig. 10). Although vertical profiles of the aerosol components are small, there are strong vertical gradients in NO_x concentrations, and for this reason we consider the comparison with the total NO_x column more reflective of overall NO_x chemistry than the ground level NO_x VMR.

Figure 10 shows that total sulphate VMR (Fig. 10a) and NO_x total column (Fig. 10c) are significantly higher over NCP region than IGP. Similarly, total ammonium VMR (Fig. 10b) is significantly larger over NCP than IGP indicating how a higher fraction of the gaseous ammonia is transformed to form ammonium over NCP region. In addition, Fig. 10d shows higher estimated levels of ammonium nitrate in MOZART-4 over NCP, reflective of the higher NOx emissions in this region. As a consequence of the different SO_2 and NO_x sources, gaseous NH_3 is more quickly removed from atmosphere over East Asia with residence time of approximately 6 hours (Fig. S5 in the Supplement) (higher values indicates lower mean residence time), which is reflected in the higher VMR of ammonium, sulphate and ammonium nitrate (Fig. 10a, b and d). It can be seen that NH_3/NH_4^+ ratio denotes lower values 0-1 (Fig. S2 in the Supplement) over East Asia than South Asia suggesting NH_4^+ partitioning is more over East Asia. As a result the NH_3 total columns over NCP are much smaller than over IGP, even though magnitude of NH_3 emission fluxes is greater over NCP that IGP.

4. Conclusion

In this work, we have compared NH_3 total columns simulated by the MOZART-4 model with IASI NH_3 satellite observations over South and East Asia. The annual mean distribution reveals a consistent spatial pattern between MOZART-4 and IASI, but MOZART-4 tends to show larger NH_3 columns over South Asia than IASI, particularly over the Indo-Gangetic Plain (IGP), whereas it is in close agreement over East Asia (including the North China Plain, NCP), with the exception of a July peak seen in the IASI dataset, which may be related to specific timing of fertilizer-related NH_3 emissions. Comparison for seasonally and monthly resolved IASI total

https://doi.org/10.5194/acp-2020-639
Preprint. Discussion started: 30 July 2020


Atmospheric Chemistry and Physics Discussions

column with the MOZART-4 simulations shows inconsistencies in spatial and temporal pattern over South Asia. This inconsistency is due to the uncertainties in emission estimate which doesn't include seasonality pattern in HTAP-v2 over South Asia, as well as uncertainties in the processing of the IASI data. Both the MOZART-4 results and IASI estimates involve assumptions that could considerably affect the comparison between total columns of NH_3.

Comparison with estimates from a ground based NH_3 monitoring network for both South and East Asia, our results showed that MOZART-4 systematically gives smaller NH_3 concentration estimates than the monitoring network. The NH_3 measurement sites used in present study mostly represent urban locations and model may not be able to capture actual concentration at point location due to coarser grid resolution over India. In addition, further assessment is needed to demonstrate the reliability of the NH_3 measurement technique used in the monitoring network, where NH_3 is measured by difference with NO_x concentrations, which may be uncertain in urban areas with high NO_x concentrations.

Despite the high NH_3 emission over both South and East Asia, a larger NH_3 total column is observed over South Asia in both the IASI and MOZART-4 estimates. This difference is explained by the MOZART-4 simulation, which treat the full atmospheric chemistry interaction with SO_2 and NO_x emissions, leading to aerosol formation. The MOZART-4 model showed higher sulphate volume mixing ratio and NO_x total column over East Asia, especially in the NCP, which is reflected in ammonium aerosol volume mixing ratio (VMR) over East Asia. This suggests that the formation of ammonium aerosols (dominated by ammonium, sulphate and ammonium nitrate) is quicker over East Asia than in South Asia, leading to lower NH_3 total columns in East Asia.

To examine the present findings future studies should investigate the effect of changing emissions of NO_x and SO_2 on NH_3 columns, for example by using perturbation of these emissions through counterfactual modeling scenarios. The comparison between model simulations using MOZART-4, satellite derived estimates from IASI and ground-based monitoring of NH_3 concentrations has highlighted the known uncertainties in emissions, satellite retrievals and measurements at point locations. In order to reduce the uncertainties in ammonia emission, it would be a key to create an NH_3 emission inventory specifically over South Asia, which is now currently under development as part of the GCRF South Asian Nitrogen Hub. This includes work to improve the bottom-up NH_3 emission inventory, taking into account primary agricultural statistics on fertilizer use and animal number distributions. There is also potential for top-down (inverse modelling) for NH_3 and NO_x by taking inference from the model, satellite and ground-based evidence. Here it is essential to recognize the need for more ground-based observational sites to measure NH_3 air concentrations in rural areas where agriculture activity is predominant. Such measurements at present are currently almost entirely absent for South Asia. Coarser global models fail to resolve the local-scale emissions, hence higher resolution regional models with advance chemistry are also needed to resolve the sources and chemical processes on urban and rural scales.

Data availability

The $0.1^{\circ} \times 0.1^{\circ}$ emission grid maps can be downloaded from the EDGAR website on https://edgar.jrc.ec.europa.eu/htap_v2/index.php?SECURE=_123 per year per sector. The model data can be downloaded upon request from the AeroCom database (http://www.htap.org/, last accessed June 22, 2020) (TF HTAP, 2018). The model data is available at Prithvi (IITM) super-computer and can be provided upon request

https://doi.org/10.5194/acp-2020-639
Preprint. Discussion started: 30 July 2020


Atmospheric Chemistry and Physics Discussions

to corresponding author. The morning overpass NH_3 total columns measured through IASI can be accessed from data center at http://cds-espri.ipsl.upmc.fr/etherTypo/index.php?id=1700&L=1. For India, ground based hourly NH_3 measurements can be obtained from CPCB website on https://app.cpcbccr.com/ccr. For China, ground based monthly mean NH_3 datasets can be downloaded from https://figshare.com/articles/Data_Descriptor_Xu_et_al_20181211_Scientific_data_docx/7451357.

Author contributions

All authors contributed to the research; SDG designed the research; PVP conducted the research; PVP and SDG wrote the paper; CJ and DS performed the MOZART model simulations; AM and MAS formulated the research; MVD, LC and PFC performed the IASI experiments; SK, DML, XL, WU, JJ, and TKA contributed to writing.

Competing interests

The authors declare that they have no conflict of interest.

Acknowledgments

We wish to thank the National Centre for Atmospheric Research (NCAR), funded by the U.S. National Science Foundation and operated by the University Corporation for Atmospheric Research, for access to the MOZART-4. All model runs were carried out on a Prithvi IBM High Performance Computing system at the Indian Institute of Tropical Meteorology (IITM), Pune India. We thank the Director, IITM for providing all the essential facilities required to complete the work. We wish to acknowledge the availability of CPCB data from CPCB webportal (https://app.cpcbccr.com/ccr). Research at ULB has been supported by the Belgian State Federal Office for Scientific, Technical and Cultural Affairs (Prodex arrangement IASI.FLOW). L.C. and M.V.D are respectively research associate and postdoctoral researcher with the Belgian F.R.S-FNRS. Cooperation between IITM and CEH has been facilitated through the NEWS India-UK Virtual Joint Centre, supported at CEH by the Biotechnological and Biological Sciences Research Council, and the Natural Environment Research Council of UK Research and Innovation (UKRI), and through the UKRI Global Challenges Research Fund (GCRF) South Asian Nitrogen Hub. The Nationwide Nitrogen Deposition Monitoring Network (NNDMN) of China was supported by the Chinese National Natural Science Foundation (41425007) and the Chinese National Research Program for Key Issues in Air Pollution Control (DQGG0208).

Financial support

This research has been supported by “Urban modeling C-DAC” sponsored project.

References

Alexandratos, N. and Bruinsma, J.: WORLD AGRICULTURE TOWARDS 2030 / 2050 The 2012 Revision. Global Perspective Studies Team, FAO Agricultural Development Economics Division. ESA Working Paper

https://doi.org/10.5194/acp-2020-639
Preprint. Discussion started: 30 July 2020

Atmospheric Chemistry and Physics Discussions

500 No. 12-03, , (12) [online] Available from: http://www.fao.org/docrep/016/ap106e/ap106e.pdf, 2012.
501 Aneja, V. P., Murray, G. C. and Southerland, J.: Atmospheric nitrogen compounds: Emissions, transport,
502 transformation, deposition, and assessment, EM Air Waste Manag. Assoc. Mag. Environ. Manag., 22–25, 1998.
503 Aneja, V. P., Battye, W., Behera, S. N., Erisman, J. W., Schlesinger, W. H. and Sharma, M.: Reactive nitrogen
504 emissions from crop and livestock farming in India, Atmos. Environ., 47, 92–103,
505 doi:10.1016/j.atmosenv.2011.11.026, 2011.
506 Anon: Central Pollution Control Board (2020), [online] Available from: https://cpcb.nic.in/quality-assurance-
507 quality-control/ (Accessed 26 May 2020), n.d.
508 Behera, S. N., Sharma, M., Aneja, V. P. and Balasubramanian, R.: Ammonia in the atmosphere: a review on
509 emission sources, atmospheric chemistry and deposition on terrestrial bodies, Environ. Sci. Pollut. Res., 20(11),
510 8092–8131, doi:10.1007/s11356-013-2051-9, 2013.
511 Chan, K. L.: Biomass burning sources and their contributions to the local air quality in Hong Kong, Sci. Total
512 Environ., 596–597, 212–221, doi:10.1016/j.scitotenv.2017.04.091, 2017.
513 Clarisse, L., Clerbaux, C., Dentener, F., Hurtmans, D. and Coheur, P. F.: Global ammonia distribution derived
514 from infrared satellite observations, Nat. Geosci., 2(7), 479–483, doi:10.1038/ngeo551, 2009.
515 Clarisse, L., Shephard, M. W., Dentener, F., Hurtmans, D., Cady-Pereira, K., Karagulian, F., Van Damme, M.,
516 Clerbaux, C. and Coheur, P. F.: Satellite monitoring of ammonia: A case study of the San Joaquin Valley, J.
517 Geophys. Res. Atmos., 115(13), 1–15, doi:10.1029/2009JD013291, 2010.
518 Clarisse, L., Van Damme, M., Clerbaux, C. and Coheur, P. F.: Tracking down global NH3 point sources with
519 wind-adjusted superresolution, Atmos. Meas. Tech., 12(10), 5457–5473, doi:10.5194/amt-12-5457-2019, 2019.
520 Clerbaux, C., Boynard, A., Clarisse, L., George, M., Hadji-Lazaro, J., Herbin, H., Hurtmans, D., Pommier, M.,
521 Razavi, A., Turquety, S., Wespes, C. and Coheur, P. F.: Monitoring of atmospheric composition using the
522 thermal infrared IASI/MetOp sounder, Atmos. Chem. Phys., 9(16), 6041–6054, doi:10.5194/acp-9-6041-2009,
523 2009.
524 Van Damme, M., Whitburn, S., Clarisse, L., Clerbaux, C., Hurtmans, D. and Coheur, P.-F.: Version 2 of the
525 IASI NH₃ neural network retrieval algorithm; near-real time and reanalysed datasets,
526 Atmos. Meas. Tech. Discuss., 1–14, doi:10.5194/amt-2017-239, 2017.
527 Van Damme, M., Clarisse, L., Whitburn, S., Hadji-Lazaro, J., Hurtmans, D., Clerbaux, C. and Coheur, P. F.:
528 Industrial and agricultural ammonia point sources exposed, Nature, 564(7734), 99–103, doi:10.1038/s41586-
529 018-0747-1, 2018.
530 Van Damme, Wichink Kruit, R. J., Schaap, M., Clarisse, L., Clerbaux, C., Coheur, P. F., Dammers, E., Dolman,
531 A. J. and Erisman, J. W.: Evaluating 4 years of atmospheric ammonia (NH3) over Europe using IASI satellite
532 observations and LOTOS-EUROS model results, J. Geophys. Res., 119(15), 9549–9566,
533 doi:10.1002/2014JD021911, 2014a.
534 Van Damme, M.Hurtmans, D., Coheur, P. F., Clerbaux, C., Dolman, A. J., Erisman, J. W., Clarisse, L., Ngadi,
535 Y. and Heald, C. L.: Global distributions, time series and error characterization of atmospheric ammonia (NH3)
536 from IASI satellite observations, Atmos. Chem. Phys., 14(6), 2905–2922, doi:10.5194/acp-14-2905-2014,
537 2014b.
538 Van Damme, Erisman, J. W., Clarisse, L., Dammers, E., Whitburn, S., Clerbaux, C., Dolman, A. J. and Coheur,
539 P.: Worldwide spatiotemporal atmospheric ammonia (NH 3), Geophys. Res. Lett., 1–9,

https://doi.org/10.5194/acp-2020-639
Preprint. Discussion started: 30 July 2020

Atmospheric Chemistry and Physics Discussions

doi:10.1002/2015GL065496.We, 2015.

Dammers, E., McLinden, C. A., Griffin, D., Shephard, M. W., Van Der Graaf, S., Lutsch, E., Schaap, M., Gainairu-Matz, Y., Fioletov, V., Van Damme, M., Whitburn, S., Clarisse, L., Cady-Pereira, K., Clerbaux, C., Francois Coheur, P. and Erisman, J. W.: NH3 emissions from large point sources derived from CrIS and IASI satellite observations, Atmos. Chem. Phys., 19(19), 12261–12293, doi:10.5194/acp-19-12261-2019, 2019.

Emmons, L. K., Walters, S., Hess, P. G., Lamarque, J. F., Pfister, G. G., Fillmore, D., Granier, C., Guenther, A., Kinnison, D., Laepple, T., Orlando, J., Tie, X., Tyndall, G., Wiedinmyer, C., Baughcum, S. L. and Kloster, S.: Description and evaluation of the Model for Ozone and Related chemical Tracers, version 4 (MOZART-4), Geosci. Model Dev., 3(1), 43–67, doi:10.5194/gmd-3-43-2010, 2010.

Fertlizer Association of India annual report 2018-19: Fertlizer Association of India annual report 2018-19., 2018.

Ghude, S. D., Fadnavis, S., Beig, G., Polade, S. D. and van der A, R. J.: Detection of surface emission hot spots, trends, and seasonal cycle from satellite-retrieved NO_2 over India, J. Geophys. Res., 113(D20), D20305, doi:10.1029/2007JD009615, 2008.

Ghude, S. D., Lal, D. M., Beig, G., van der A, R. and Sable, D.: Rain-Induced Soil NO_x Emission From India During the Onset of the Summer Monsoon: A Satellite Perspective, J. Geophys. Res., 115(D16), D16304, doi:10.1029/2009JD013367, 2010.

Ghude, S. D., Beig, G., Kulkarni, P. S., Kanawade, V. P., Fadnavis, S., Remedios, J. J. and Kulkarni, S. H.: Regional co pollution over the Indian-subcontinent and various transport pathways as observed by mopitt, Int. J. Remote Sens., 32(21), 6133–6148, doi:10.1080/01431161.2010.507796, 2011.

Ghude, S. D., Kulkarni, S. H., Jena, C., Pfister, G. G., Beig, G., Fadnavis, S. and Van Der, R. J.: Application of satellite observations for identifying regions of dominant sources of nitrogen oxides over the indian subcontinent, J. Geophys. Res. Atmos., 118(2), 1075–1089, doi:10.1029/2012JD017811, 2013.

Ghude, S. D., Chate, D. M., Jena, C., Beig, G., Kumar, R., Barth, M. C., Pfister, G. G., Fadnavis, S. and Pithani, P.: Premature mortality in India due to $PM_{2.5}$ and ozone exposure, Geophys. Res. Lett., 43(9), 4650–4658, doi:10.1002/2016GL068949, 2016.

Huang, K., Fu, J. S., Hsu, N. C., Gao, Y., Dong, X., Tsay, S. C. and Lam, Y. F.: Impact assessment of biomass burning on air quality in Southeast and East Asia during BASE-ASIA, Atmos. Environ., 78(2012), 291–302, doi:10.1016/j.atmosenv.2012.03.048, 2013.

Huang, X., Song, Y., Li, M., Li, J., Huo, Q., Cai, X., Zhu, T., Hu, M. and Zhang, H.: A high-resolution ammonia emission inventory in China, Global Biogeochem. Cycles, 26(1), 1–14, doi:10.1029/2011GB004161, 2012.

Janssens-Maenhout G., Dentener F., Van Aardenne J., Monni S., Pagliari V., Orlandini L., Klimont Z., Kurokawa J., Akimoto H., Ohara T., Wankmueller R., Battye B., Grano D., Zuber A., K. T. .: EDGAR-HTAP: a Harmonized Gridded Air Pollution Emission Dataset Based on National Inventories, Ispra (Italy): European Commission Publications Office, , (February), 1–18, doi:ISBN 978-92-79-23122-0, ISSN 1831-9424, 2012.

Janssens-Maenhout, G., Dentener, F. J., Aardenne, J. Van, Monni, S., Pagliari, V., Orlandini, L., Klimont, Z., Kurokawa, J., Akimoto, H., Ohara, T., Wankmüller, R., Battye, B., Grano, D., Zuber, A. and Keating, T.: EDGAR-HTAP: a harmonized gridded air pollution emission dataset based on national inventories., 2012.

Janssens-Maenhout, G., Koffi, B., Crippa, M., Pouliot, G., Zhang, Q., Wankmüller, R., Frost, G., Dentener, F.,

https://doi.org/10.5194/acp-2020-639
Preprint. Discussion started: 30 July 2020

Atmospheric Chemistry and Physics Discussions

580 Li, M., Guizzardi, D., Denier van der Gon, H., Darras, S., Kuenen, J. J. P., Keating, T., Klimont, Z., Kurokawa,
581 J. and Muntean, M.: HTAP_v2.2: a mosaic of regional and global emission grid maps for 2008 and 2010 to
582 study hemispheric transport of air pollution, Atmos. Chem. Phys., 15(19), 11411–11432, doi:10.5194/acp-15-
583 11411-2015, 2015.
584 Jena, C., Ghude, S. D., Pfister, G. G., Chate, D. M., Kumar, R., Beig, G., Surendran, D. E., Fadnavis, S. and Lal,
585 D. M.: Influence of springtime biomass burning in South Asia on regional ozone (O3): A model based case
586 study, Atmos. Environ., 100, 37–47, doi:10.1016/j.atmosenv.2014.10.027, 2015.
587 Kumar, R., Barth, M. C., Pfister, G. G., Delle Monache, L., Lamarque, J. F., Archer-Nicholls, S., Tilmes, S.,
588 Ghude, S. D., Wiedinmyer, C., Naja, M. and Walters, S.: How Will Air Quality Change in South Asia by 2050?,
589 J. Geophys. Res. Atmos., 123(3), 1840–1864, doi:10.1002/2017JD027357, 2018.
590 Kurokawa, J., Ohara, T., Morikawa, T., Hanayama, S., Janssens-Maenhout, G., Fukui, T., Kawashima, K. and
591 Akimoto, H.: Emissions of air pollutants and greenhouse gases over Asian regions during 2000-2008: Regional
592 Emission inventory in ASia (REAS) version 2, Atmos. Chem. Phys., 13(21), 11019–11058, doi:10.5194/acp-13-
593 11019-2013, 2013.
594 Lal, D. M., Ghude, S. D., Singh, J. and Tiwari, S.: Relationship between Size of Cloud Ice and Lightning in the
595 Tropics, , doi:10.1155/2014/471864, 2014.
596 Li, L., Friedl, M. A., Xin, Q., Gray, J., Pan, Y. and Frolking, S.: Mapping Crop Cycles in China Using MODIS-
597 EVI Time Series, , (September), doi:10.3390/rs6032473, 2014.
598 Li, M., Zhang, Q., Kurokawa, J., Woo, J., He, K. B., Lu, Z. and Ohara, T.: MIX : a mosaic Asian anthropogenic
599 emission inventory for the MICS-Asia and the HTAP projects, , 34813–34869, doi:10.5194/acpd-15-34813-
600 2015, 2015.
601 Li, M., Zhang, Q., Kurokawa, J. I., Woo, J. H., He, K., Lu, Z., Ohara, T., Song, Y., Streets, D. G., Carmichael,
602 G. R., Cheng, Y., Hong, C., Huo, H., Jiang, X., Kang, S., Liu, F., Su, H. and Zheng, B.: MIX: A mosaic Asian
603 anthropogenic emission inventory under the international collaboration framework of the MICS-Asia and
604 HTAP, Atmos. Chem. Phys., 17(2), 935–963, doi:10.5194/acp-17-935-2017, 2017.
605 Liu, L., Zhang, X., Xu, W., Liu, X., Li, Y., Lu, X., Zhang, Y. and Zhang, W.: Temporal characteristics of
606 atmospheric ammonia and nitrogen dioxide over China based on emission data, satellite observations and
607 atmospheric transport modeling since 1980, Atmos. Chem. Phys., 17(15), 9365–9378, doi:10.5194/acp-17-
608 9365-2017, 2017a.
609 Liu, X., Xu, W., Duan, L., Du, E., Pan, Y., Lu, X., Zhang, L., Wu, Z., Wang, X., Zhang, Y., Shen, J., Song, L.,
610 Feng, Z., Liu, X., Song, W., Tang, A., Zhang, Y., Zhang, X. and Collett, J. L.: Atmospheric Nitrogen Emission,
611 Deposition, and Air Quality Impacts in China: an Overview, Curr. Pollut. Reports, 3(2), 65–77,
612 doi:10.1007/s40726-017-0053-9, 2017b.
613 Metzger, S., Dentener, F., Pandis, S. and Lelieveld, J.: Gas/aerosol partitioning: 1. A computationally efficient
614 model, J. Geophys. Res. Atmos., 107(16), doi:10.1029/2001JD001102, 2002.
615 Pinder, R. W., Adams, P. J. and Pandis, S. N.: Ammonia Emission Controls as a Cost-Effective Strategy for
616 Reducing Atmospheric Particulate Matter in the Eastern United States, Environ. Sci. Technol., 41(2), 380–386,
617 doi:10.1021/es060379a, 2007.
618 Pinder, R. W., Gilliland, A. B. and Dennis, R. L.: Environmental impact of atmospheric NH3 emissions under
619 present and future conditions in the eastern United States, Geophys. Res. Lett., 35(12),

https://doi.org/10.5194/acp-2020-639
Preprint. Discussion started: 30 July 2020

doi:10.1029/2008GL033732, 2008.

Pollution, C. and Board, C.: Guidelines for Manual Sampling & Analyses, 2011.

Randerson, J., Werf, G. Van Der, Giglio, L., DAAC, G. C.-O. and 2015, undefined: Global Fire Emissions Database, Version 4.1 (GFEDv4), daac.ornl.gov [online] Available from: https://daac.ornl.gov/cgi-bin/download.pl?ds_id=1293&source=schema_org_metadata (Accessed 26 May 2020), n.d.

Seinfeld, J. H. and Pandis, S. N.: Atmospheric Chemistry and Physics: From Air Pollution to Climate Change, Wiley. [online] Available from: https://books.google.co.in/books?id=J3s30hwn_K0C, 2012.

Seinfeld, J. H., Pandis, S. N. and Noone, K.: Atmospheric Chemistry and Physics: From Air Pollution to Climate Change , Phys. Today, 51(10), 88–90, doi:10.1063/1.882420, 1998.

Sharma, C., Tiwari, M. K. and Pathak, H.: Estimates of emission and deposition of reactive nitrogenous species for India, Curr. Sci., 94(11), 1439–1446, 2008.

Sharma, S. K., Harit, R. C., Kumar, V., Mandal, T. K. and Pathak, H.: Ammonia Emission from Rice-Wheat Cropping System in Subtropical Soil of India, Agric. Res., 3(2), 175–180, doi:10.1007/s40003-014-0107-9, 2014a.

Sharma, S. K., Kumar, M., Rohtash, Gupta, N. C., Saraswati, Saxena, M. and Mandal, T. K.: Characteristics of ambient ammonia over Delhi, India., 2014b.

Surendran, D., Jena, C., Beig, G., Chate, D. M. and Ghude, S. D.: Quantifying the sectoral contribution of pollution transport from South Asia during summer and winter monsoon seasons in support of HTAP-2 experiment, Atmos. Environ., 145, 60–71, doi:10.1016/j.atmosenv.2016.09.011, 2016.

Surendran, D. E., Ghude, S. D., Beig, G., Emmons, L. K., Jena, C., Kumar, R., Pfister, G. G. and Chate, D. M.: Air quality simulation over South Asia using Hemispheric Transport of Air Pollution version-2 (HTAP-v2) emission inventory and Model for Ozone and Related chemical Tracers (MOZART-4), Atmos. Environ., 122, 357–372, doi:10.1016/j.atmosenv.2015.08.023, 2015.

Sutton, M. A., Reis, S., Riddick, S. N., Dragosits, U., Nemitz, E., Theobald, M. R., Tang, Y. S., Braban, C. F., Vieno, M., Dore, A. J., Mitchell, R. F., Wanless, S., Daunt, F., Fowler, D., Blackall, T. D., Milford, C., Flechard, C. R., Loubet, B., Massad, R., Cellier, P., Personne, E., Coheur, P. F., Clarisse, L., Van Damme, M., Ngadi, Y., Clerbaux, C., Skjøth, C. A., Geels, C., Hertel, O., Kruit, R. J. W., Pinder, R. W., Bash, J. O., Walker, J. T., Simpson, D., Horváth, L., Misselbrook, T. H., Bleeker, A., Dentener, F. and de Vries, W.: Towards a climate-dependent paradigm of ammonia emission and deposition, Philos. Trans. R. Soc. B Biol. Sci., 368(1621), 20130166–20130166, doi:10.1098/rstb.2013.0166, 2013.

Sutton, M. A., J. Drewer, A. Moring, T.K Adhya, A. Ahmed and A. Bhatia: The Indian nitrogen assessment : sources of reactive nitrogen, environmental and climate effects, management options, and policies, in The Indian Nitrogen Assessment, edited by Y. P. Abrol, T. K. Adhya, V. P. Aneja, N. Raghuram, H. Pathak, U. Kulshrestha, C. Sharma, and B. Singh, pp. 9–25, Elsevier., 2017.

Wesely, M. L.: Parameterization of surface resistances to gaseous dry deposition in regional-scale numerical models, Atmos. Environ., 23(6), 1293–1304, doi:10.1016/0004-6981(89)90153-4, 1989.

Whitburn, S., Damme, M. Van, Clarisse, L., Bauduin, S., Heald, C. L., Hurtmans, D., Zondlo, M. A., Clerbaux, C. and Coheur, P.: A flexible and robust neural network IASI-NH 3, , 6581–6599, doi:10.1002/2016JD024828.Received, 2016.

Wu, J., Kong, S., Wu, F., Cheng, Y., Zheng, S., Yan, Q., Zheng, H., Yang, G., Zheng, M., Liu, D., Zhao, D. and

https://doi.org/10.5194/acp-2020-639
Preprint. Discussion started: 30 July 2020

Atmospheric Chemistry and Physics Discussions

660 Qi, S.: Estimating the open biomass burning emissions in central and eastern China from 2003 to 2015 based on
661 satellite observation, Atmos. Chem. Phys., 18(16), 11623–11646, doi:10.5194/acp-18-11623-2018, 2018.
662 Xu, R. T., Pan, S. F., Chen, J., Chen, G. S., Yang, J., Dangal, S. R. S., Shepard, J. P. and Tian, H. Q.: Half-
663 Century Ammonia Emissions From Agricultural Systems in Southern Asia: Magnitude, Spatiotemporal
664 Patterns, and Implications for Human Health, GeoHealth, 2(1), 40–53, doi:10.1002/2017gh000098, 2018.
665 Xu, W., Zhang, L. and Liu, X.: A database of atmospheric nitrogen concentration and deposition from the
666 nationwide monitoring network in China, , (December 2018), 2–7, 2019.
667 Zhang, X., Liu, J., Han, H., Zhang, Y., Jiang, Z., Wang, H., Meng, L., Li, Y. C. and Liu, Y.: Satellite-Observed
668 Variations and Trends in Carbon Monoxide over Asia and Their Sensitivities to Biomass Burning, Remote
669 Sens., 12(5), 830, doi:10.3390/rs12050830, 2020.
670 Zhao, B., Wang, S. X., Liu, H., Xu, J. Y., Fu, K., Klimont, Z., Hao, J. M., He, K. B., Cofala, J. and Amann, M.:
671 NOx emissions in China: Historical trends and future perspectives, Atmos. Chem. Phys., 13(19), 9869–9897,
672 doi:10.5194/acp-13-9869-2013, 2013.
673 Zheng, J., Hu, M., Du, Z., Shang, D., Gong, Z., Qin, Y., Fang, J., Gu, F., Li, M., Peng, J., Li, J., Zhang, Y.,
674 Huang, X., He, L., Wu, Y. and Guo, S.: Influence of biomass burning from South Asia at a high-altitude
675 mountain receptor site in China, Atmos. Chem. Phys., 17(11), 6853–6864, doi:10.5194/acp-17-6853-2017,
676 2017.
677 Zhou, Y., Zhang, Y., Tian, D. and Mu, Y.: Impact of dicyandiamide on emissions of nitrous oxide, nitric oxide
678 and ammonia from agricultural field in the North China Plain, J. Environ. Sci. (China), 40, 20–27,
679 doi:10.1016/j.jes.2015.08.016, 2016.
680 Zhu, L., Henze, D. K., Bash, J. O., Cady-Pereira, K. E., Shephard, M. W., Luo, M. and Capps, S. L.: Sources
681 and Impacts of Atmospheric NH3: Current Understanding and Frontiers for Modeling, Measurements, and
682 Remote Sensing in North America, Curr. Pollut. Reports, 1(2), 95–116, doi:10.1007/s40726-015-0010-4, 2015.
683
684
685
686
687
688
689
690
691
692
693
694
695
696
697
698
699

https://doi.org/10.5194/acp-2020-639
Preprint. Discussion started: 30 July 2020

Atmospheric Chemistry and Physics Discussions

FIGURE CAPTIONS

Figure 1. Spatial distribution of total NH_3 emissions ($\times10^{10}$ kg $m^{-2}s^{-1}$) over Asia. Data are shown at 0.1° × 0.1° grid resolution from Hemispheric Transport of Air Pollution version-2 (HTAP-v2) emission inventory. The solid rectangles indicate the Indo-Gangetic plain, IGP (20°N-32°N, 70°E-95°E) and the North China Plain, NCP (30°N-40°N, 110°E-120°E).

Figure 2. Monthly variation of anthropogenic (HTAP-v2) (molecules cm^{-2} s^{-1}) (top), Biomass Burning (GEFED-v3) (molecules cm^{-2} s^{-1}) (middle) and Soil (CESM) (molecules cm^{-2} s^{-1}) (bottom) NH_3 emission averaged from Indo-Gangetic plain (20°N-32°N, 70°E-95°E) and the North China Plain (30°N-40°N, 110°E-120°E).

Figure 3. Geographical locations of surface NH_3 observational sites (69 locations) from the air quality automatic monitoring network operated by the Central Pollution Control Board (CPCB, 2020), India and observational sites (32 locations) from Nationwide Nitrogen Deposition Monitoring Network (NNDMN) operated by China Agricultural University, China.

Figure 4. Spatial distributions annual mean NH_3 ($\times10^{16}$ molecules cm^{-2}) total columns over Asia for the year 2010. (a) Simulated by MOZART-4, (b) from the IASI satellite observations and (c) spatial difference between MOZART-4 and IASI.

Figure 5. (a) Scatter plot between annual averaged IASI and MOZART-4 simulated NH_3 ($\times10^{16}$ molecules cm^{-2}) total columns over IGP, South Asia (rectangle: 20°N-32°N, 70°E-95°E) and (b) Scatter plot between annual averaged IASI and MOZART-4 simulated NH_3 ($\times10^{16}$ molecules cm^{-2}) total columns over NCP, East Asia (rectangle: 30°N-40°N, 110°E-120°E).

Figure 6. Seasonal NH_3 total columns distribution ($\times10^{16}$ molecules cm^{-2}) in 2010 (left) simulated by MOZART-4, (middle) measured by IASI satellite and (right) spatial differences between MOZART-4 and IASI during (top to bottom) winter (DJF) spring (MAM) summer (JJA) and autumn (SON) seasons.

Figure 7. (a) Comparison between monthly averaged IASI and MOZART-4 simulated NH_3 ($\times10^{16}$ molecules cm^{-2}) total columns over IGP South Asia (20°N-32°N, 70°E-95°E), (b) Comparison of monthly averaged IASI and MOZART-4 simulated NH_3 ($\times10^{16}$ molecules cm^{-2}) total columns over NCP East Asia (30°N-40°N, 110°E-120°E) (bar indicates standard error of 88 and 35 pixels in IGP and NCP respectively).

Figure 8. (a) Scatter plot between annual averaged surface observations from 69 monitoring sites (Fig. 2) over South Asia and MOZART-4 simulated surface NH_3 (µg m^{-3}) (992 hPa) interpolated at the locations of 69 sites (b) Comparison between monthly mean surface observations from 69 monitoring sites and MOZART-4 simulated monthly mean NH_3 (µg m^{-3}) concentration interpolated at the locations of 69 sites over South Asia.

https://doi.org/10.5194/acp-2020-639
Preprint. Discussion started: 30 July 2020

Atmospheric Chemistry and Physics Discussions

740

741 **Figure 9. (a) Scatter plot between annual averaged surface observations from 32 monitoring sites (Fig. 2)**
742 **over East Asia and MOZART-4 simulated surface NH_3 (μg m^{-3}) (992 hPa) interpolated at the locations of**
743 **32 sites (b) Comparison between monthly mean surface observations from 32 monitoring sites and**
744 **MOZART-4 simulated monthly mean NH_3 (μg m^{-3}) concentration interpolated at the locations of 32 sites**
745 **over East Asia.**

746

747 **Figure 10. MOZART-4 simulated spatial distribution of annual averaged (a) total sulphate aerosol (×10^9**
748 **ppb), (b) total Ammonium aerosol (×10^9 ppb), (c) NO_x total columns (×10^{16} molecules cm^{-2}) and (d) total**
749 **ammonium nitrate aerosol (×10^9 ppb) over Asia.**

750

751

752

753

754

755

756

757

758

759

760

761

762

763

764

765

766

767

768

769

770

771

772

773

774

775

776

777

https://doi.org/10.5194/acp-2020-639
Preprint. Discussion started: 30 July 2020

Atmospheric Chemistry and Physics Discussions

778 **TABLES**

779 **Table 1 Model performance statistics for NH_3 total columns over Asia from IASI and MOZART-4**
780 **simulations for the year 2010**

781

Statistics indicator	IGP, South Asia	NCP, East Asia
Mean (Model-IASI) ($\times 10^{16}$ molecules cm^{-2})	0.76	-0.15
Normalized Mean Bias (NMB)	0.42	-0.20
Variance ($\times 10^{16}$ molecules cm^{-2})	1.64	-1.23
Root Mean Square Error (RMSE) ($\times 10^{16}$ molecules cm^{-2})	0.125	0.041
Correlation Coefficient (r)	0.85	0.88

782
783
784
785
786
787
788
789
790
791
792
793
794
795
796
797
798
799
800
801
802
803
804
805
806
807

https://doi.org/10.5194/acp-2020-639
Preprint. Discussion started: 30 July 2020

Atmospheric Chemistry and Physics Discussions

808 **Table 2 Model performance statistics for NH_3 concentration over East and South Asia from MOZART-4**
809 **simulations and observational network for the year 2010**

810

Statistics indicator	IGP, South Asia	NCP, East Asia
Mean (Model-Observations) ($\mu g\ m^{-3}$)	-13.47	3.1
Normalized Mean Bias (NMB)	0.44	-0.46
Variance ($\mu g\ m^{-3}$)	-0.629	-0.88
Root Mean Square Error (RMSE) ($\mu g\ m^{-3}$)	1.91	0.728
Correlation Coefficient (r)	0.82	0.65

811

812

https://doi.org/10.5194/acp-2020-639
Preprint. Discussion started: 30 July 2020

Atmospheric Chemistry and Physics Discussions

Figure 1

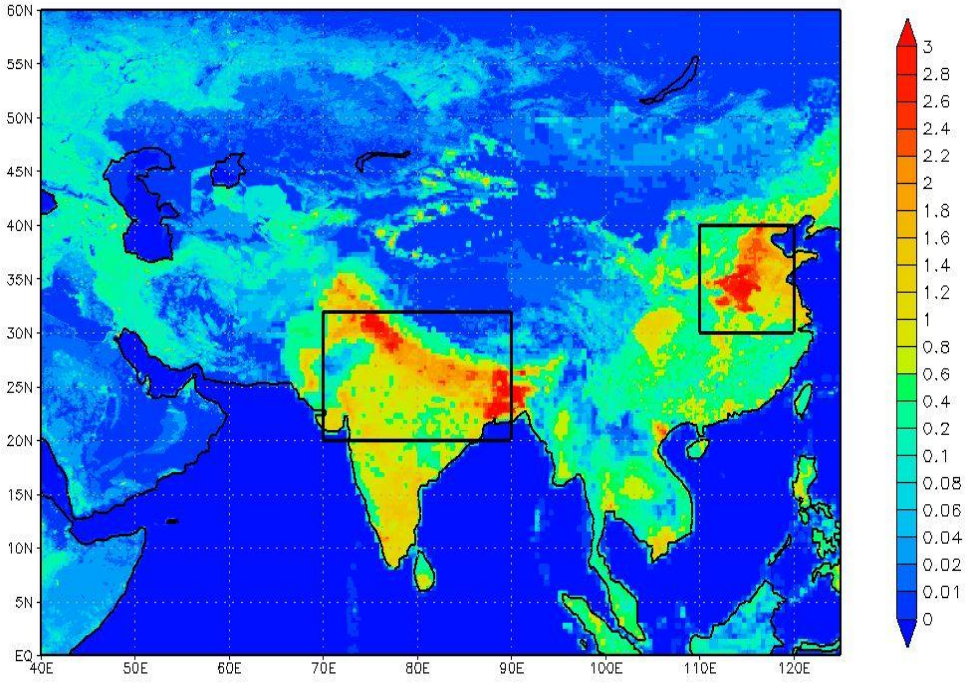

https://doi.org/10.5194/acp-2020-639
Preprint. Discussion started: 30 July 2020

Atmospheric Chemistry and Physics Discussions

832 **Figure 2**

833

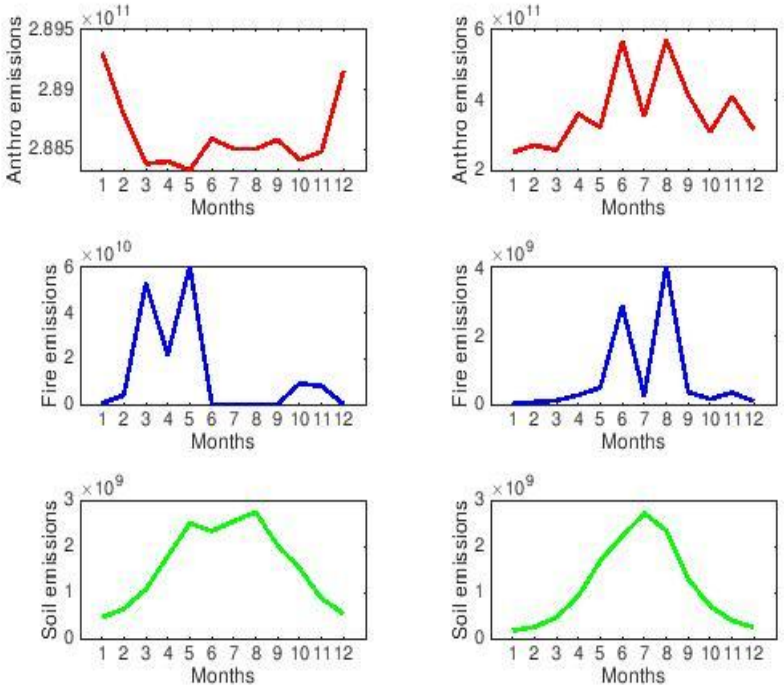

834

835

836

837

838

839

840

841

842

843

844

845

846

847

848

https://doi.org/10.5194/acp-2020-639
Preprint. Discussion started: 30 July 2020

Atmospheric Chemistry and Physics Discussions

849 **Figure 3**

850

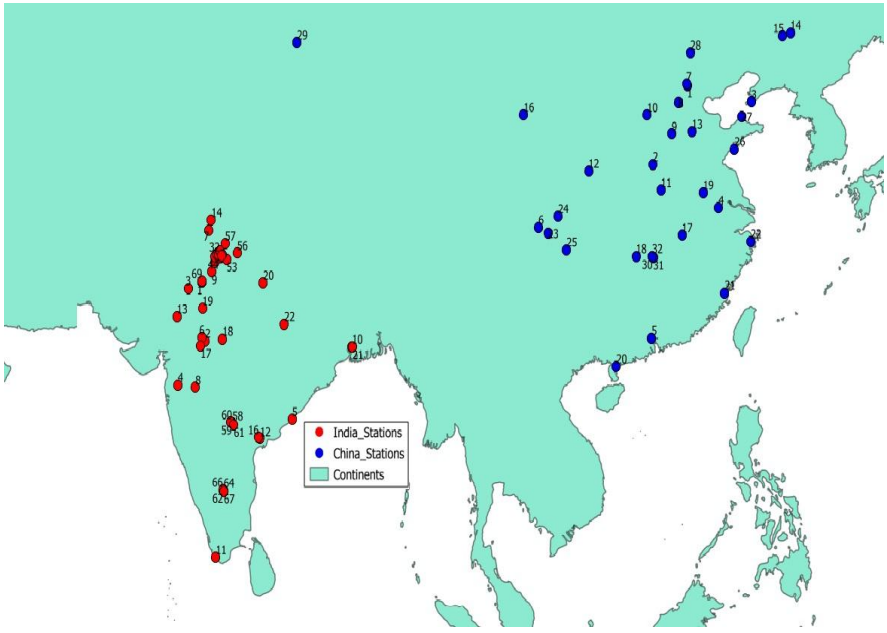

851

852

853

854

855

856

857

858

859

860

861

862

863

864

865

866

867

868

https://doi.org/10.5194/acp-2020-639
Preprint. Discussion started: 30 July 2020

Atmospheric Chemistry and Physics Discussions

869 **Figure 4**

870

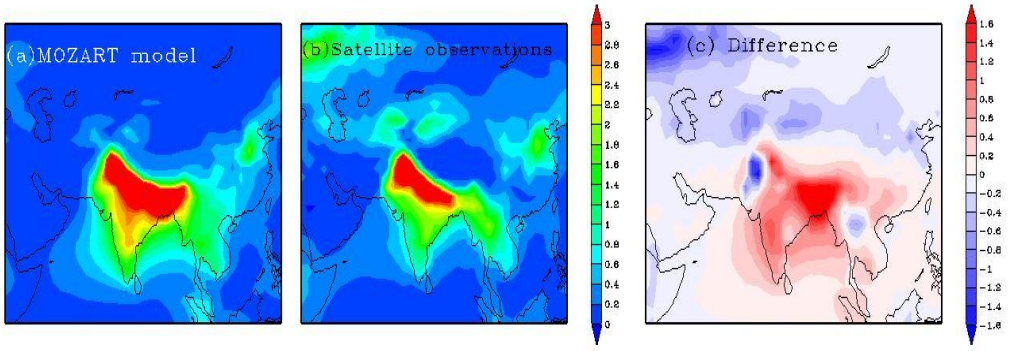

871

872

873

874

875

876

877

878

879

880

881

882

883

884

885

886

887

888

889

890

891

892

893

https://doi.org/10.5194/acp-2020-639
Preprint. Discussion started: 30 July 2020

Atmospheric Chemistry and Physics Discussions

894 **Figure 5**

895

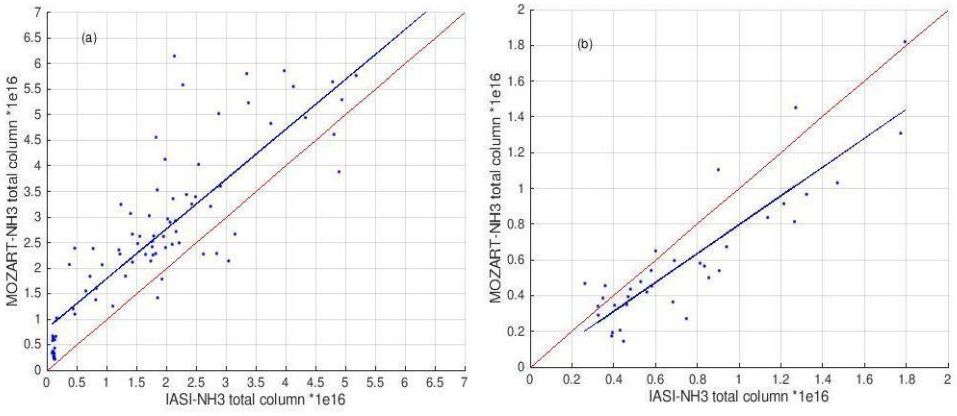

896
897
898
899
900
901
902
903
904
905
906
907
908
909
910
911
912
913
914
915
916
917
918

https://doi.org/10.5194/acp-2020-639
Preprint. Discussion started: 30 July 2020

Atmospheric Chemistry and Physics Discussions

Figure 6

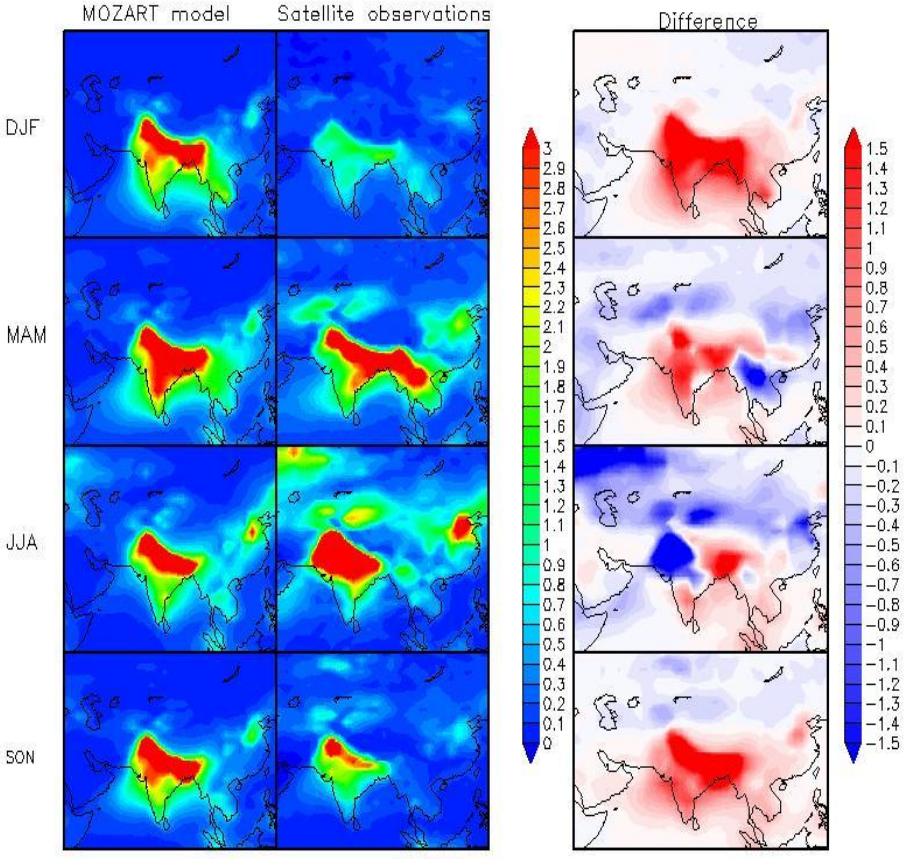

https://doi.org/10.5194/acp-2020-639
Preprint. Discussion started: 30 July 2020

Atmospheric Chemistry and Physics Discussions

Figure 7

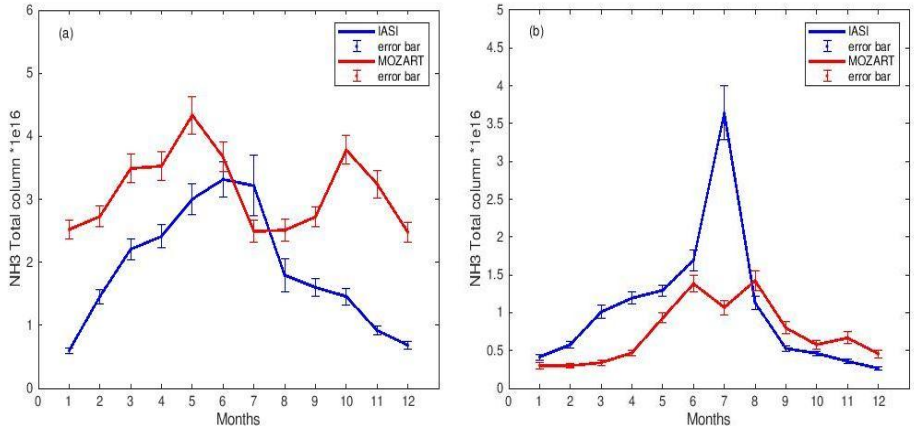

https://doi.org/10.5194/acp-2020-639
Preprint. Discussion started: 30 July 2020

Atmospheric Chemistry and Physics Discussions

957 **Figure 8**

958

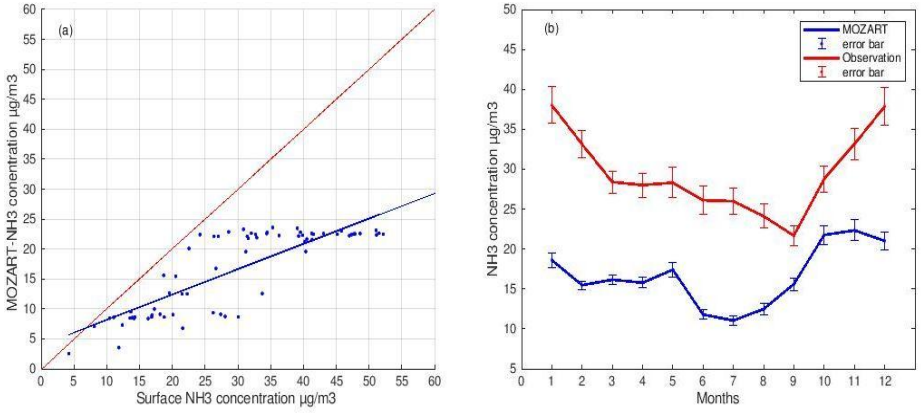

959
960
961
962
963
964
965
966
967
968
969
970
971
972
973
974
975
976
977
978
979
980
981
982
983
984
985

https://doi.org/10.5194/acp-2020-639
Preprint. Discussion started: 30 July 2020

Atmospheric Chemistry and Physics Discussions

Figure 9

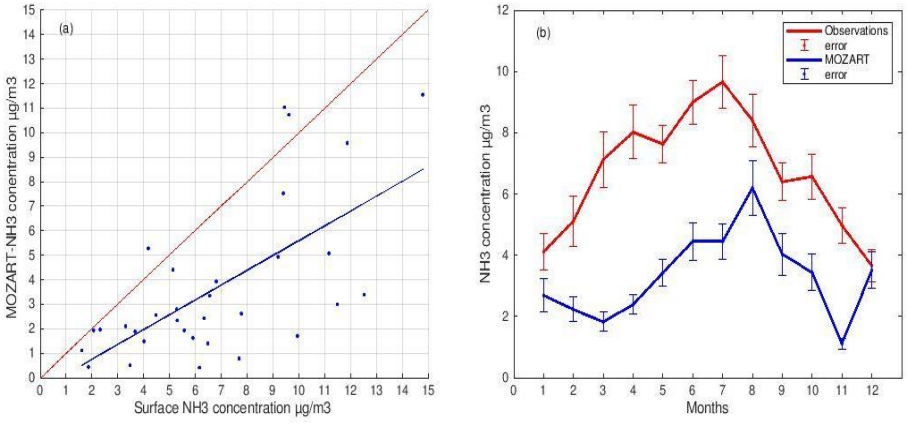

https://doi.org/10.5194/acp-2020-639
Preprint. Discussion started: 30 July 2020

Atmospheric Chemistry and Physics Discussions

Figure 10